Three-dimensional model of Hellenic Arc deformation and origin of the Cretan uplift

Athanassios Ganas[1] and Tom Parsons[2]

Received 20 January 2008; revised 28 December 2008; accepted 14 April 2009; published 20 June 2009.

[1] The Hellenic Arc of Greece is the most seismically active part of Europe, but little is know about its mechanics. We modeled deformation along the arc using a finite element model. The model was intended to capture large-scale 3-D structure of Nubian plate subduction beneath the Aegean block and its deformational consequences. The shape of the interface was developed using mapped traces at the surface and earthquake hypocenters at depth. Model block motions were constrained by recent compilations of GPS velocity vectors. We simulated a 10 ka period of convergence between Nubia and the Aegean and calculated the strain field in the overriding plate as well as the spatial distribution and orientation of differential stress ($|\sigma_1 - \sigma_3|$). From these calculations we derived testable quantities such as the expected seismic moment rate on the interplate contact, uplift pattern, and distribution of strain modes. Our relatively simple model broadly reproduced observed uplift patterns, earthquake activity, and loci of extension and contraction. The model showed a localization of uplift near the island of Crete, where the fastest Aegean uplift rates are well documented. Comparison of calculated expected seismic moment and observed earthquake catalogs implies a nearly fully coupled interplate contact. On the basis of our modeling results, we suggest that south Aegean deformation is driven primarily by the fast moving ($\sim$33 mm a^{-1}) Aegean upper plate overriding a nearly stalled ($\sim$5 mm a^{-1}) Nubian lower plate. This tectonic setting thus more closely resembles a continental thrust than it does a typical oceanic subduction zone.

Citation: Ganas, A., and T. Parsons (2009), Three-dimensional model of Hellenic Arc deformation and origin of the Cretan uplift, *J. Geophys. Res.*, *114*, B06404, doi:10.1029/2008JB005599.

1. Introduction

[2] The Hellenic Arc is part of the larger boundary zone between the Eurasia, Africa, and Arabia plates. Earthquakes in southern Greece are caused primarily by interaction between the relatively small Aegean Sea and the larger Africa (Nubia) plates. Nubia subducts beneath the Aegean Sea plate along the Hellenic Arc, from the western Peloponnese through Crete and Rhodes to western Turkey (Figure 1). The largest recent earthquakes to have occurred near the Hellenic Arc plate boundary had magnitudes of about M = 7.3 [*Ambraseys*, 2001]; historical and archeological studies have suggested that earthquakes occurred near Crete in 365 A.D. [e.g., *Stiros*, 2001] and 1303 A.D. [e.g., *Guidoboni and Comastri*, 1997] that may have been much larger (M > 8) than any Hellenic Arc earthquake of the twentieth century. A maximum magnitude calculation from catalog data suggests a M = 7.8 ± 0.4 value [*Hamouda*, 2006]. Globally, convergent plate tectonic environments similar to that of the Hellenic Arc commonly produce M > 8 earthquakes.

[3] In this paper we investigate the mechanics of Aegean-Nubian interactions to understand the following issues: (1) the expected ramifications of the 3-D geometry of the Aegean-Nubian plate interface and geodetically constrained plate rates, (2) the expected spatial distribution of seismic moment release, (3) origin of the uplift that is raising the island of Crete at high rates ($\geq$6 mm a^{-1}), and (4) how much of the complex distribution of transform, extensional, and compressional deformation in the Aegean block can be attributed to interactions with the Nubian plate.

[4] The Hellenic Arc is a key feature along the Alpine-Himalayan belt [*McKenzie*, 1972]. Its origin is linked to the northward motion of the African (Nubian) plate and has been in existence since Oligocene–lower Miocene time in what is today part of the north Aegean region [*Seyitoglu and Scott*, 1992; *Gautier et al.*, 1999; *Okay and Satir*, 2000]. Today the arc has a total length of about 1200 km from approximately 37.5°N, 20.0°E offshore the island of Zakynthos (Figure 1) to 36.0°N, 29.0°E offshore of the island of Rhodes.

[5] The active tectonics of the Hellenic Arc show a range of kinematics: E-W extension along the arc at both its edges (Peloponnese, eastern Crete and Dodecanese) [*Lyon-Caen et al.*, 1988; *Armijo et al.*, 1992; *de Chabalier et al.*, 1992;

[1]Geodynamics Institute, National Observatory of Athens, Athens, Greece.
[2]U.S. Geological Survey, Menlo Park, California, USA.

0148-0227/09/2008JB005599$09.00

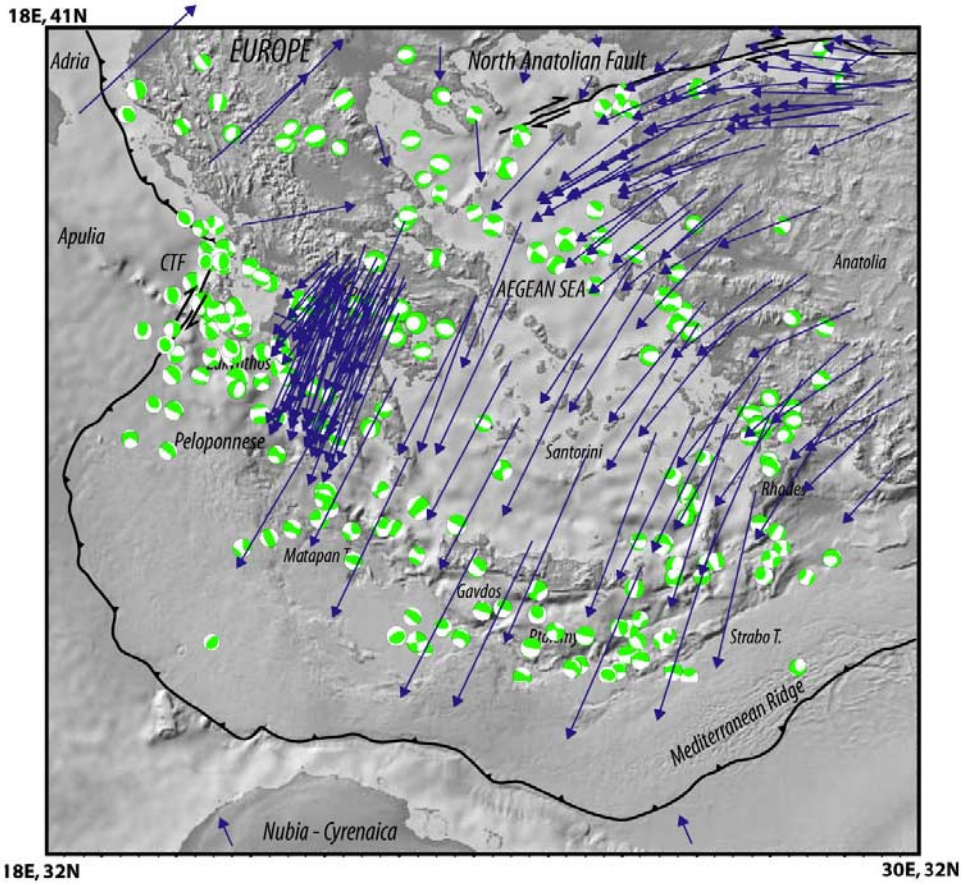

Figure 1. Relief map of the Hellenic Arc and the Aegean Sea. The surface trace of the Hellenic Arc is shown as adapted after *Kreemer and Chamot-Rooke* [2004]. Also shown are active faults (CTF stands for Cephalonia Transform Fault), GPS vectors are after *Nyst and Thatcher* [2004] and *Reilinger et al.* [2006], and selected earthquake focal mechanisms are from the Global CMT database.

Hatzfeld et al., 1993; *Kokkalas and Doutsos*, 2001], and primarily N-S (±30°) extension in the middle part [*Fassoulas*, 2001; *Caputo et al.*, 2006]. The fore-arc basin is deformed by both normal and strike-slip faults [*Angelier et al.*, 1982; *Chamot-Rooke et al.*, 2005]. The most prominent features are a series of linear, seafloor escarpments with more than 2 km of individual relief; these are often referred to as trenches, although they are not currently directly associated with subduction. Three NE-SW striking trenches have developed in the eastern part of the arc with high-angle dips to the southeast (named Ptolemy, Pliny, and Strabo and ~100–300 km long; Figure 1). The latter two accommodate 21–23 mm a^{-1} of sinistral motion [*Kreemer and Chamot-Rooke*, 2004]. A fourth trench (named Matapan, ~300 km long; Figure 1) crosses the floor of the south and central Ionian Sea, strikes on average NW-SE, and dips to the southwest.

[6] The back-arc basin has been deforming at very slow rates and is modeled as a nearly rigid block in most GPS studies [*Reilinger et al.*, 2006]. The arc terminates offshore of the island of Zakynthos, where the relative plate motion is accommodated by right-lateral shear along the Cephalonia transform fault [*Scordilis et al.*, 1985] and shortening across the Apulia escarpment. The Cephalonia transform fault is moving at a rate of 20 ± 1 mm a^{-1} [*Serpelloni et al.*, 2005]. Farther north, the Adria microplate collides with Eurasia at a ENE-WSW direction [*Anderson and Jackson*, 1987; *Battaglia et al.*, 2004].

[7] The Nubia plate advances to the NNW at a rate of about 5 mm a^{-1} [*Fernandes et al.*, 2003]. Subduction of the oceanic lithosphere is subhorizontal offshore of Cyrenaica and dips gently up to the island of Gavdos (Figure 1) where it plunges beneath Crete, defining a Benioff zone [*Papazachos et al.*, 2000a]. Focal mechanisms of earthquakes along the plate interface show mostly reverse faulting south of Crete [*Taymaz et al.*, 1990; *Bohnhoff et al.*, 2001], and a mixture of reverse-oblique mechanisms at intermediate depths [*Beißer et al.*, 1990; *Taymaz et al.*, 1990; *Benetatos et al.*, 2004]. The former type of faulting is due to N-S (across arc) compression, the latter is likely a result of E-W (along arc) compression at intermediate depths (50–170 km). There are no earthquake data from events deeper than 170 km (global CMT catalog) in agreement with the slab detachment models of *Spakman et al.* [1988], *Wortel and Spakman* [2000], and *Faccenna et al.* [2006].

[8] A complementary component of deformation that impacts the Aegean region is westward motion of the Anatolian block, which is pushed into the Aegean by continental collision in eastern Turkey–western Iran area (Figure 1) [*Jackson and McKenzie*, 1984]. This motion is on

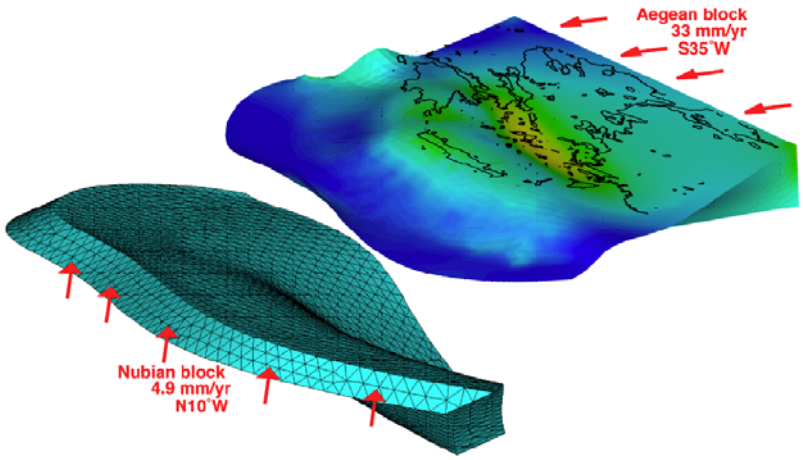

Figure 2. The two blocks of the finite element model showing the 3-D shape of the subducting Nubian slab and the applied displacement vectors. The 2-D representation (Earth's surface) is given in Figure 1. Deformation of the upper plate is shown exaggerated 100 times. Color shading is differential stress in the upper plate.

average about 21 mm a^{-1} [*Reilinger et al.*, 2006] up to the shores of the Aegean Sea. Thereafter an increase in GPS velocities is observed that is significant enough to differentiate the Anatolian from the Aegean blocks, the latter moving N215°E with a velocity of 33 mm a^{-1} [*Reilinger et al.*, 2006].

[9] In this paper we present results from a finite element model of Hellenic Arc deformation. We want to see what the implications of the interplate geometry are on uplift of Crete and other areas along the external Hellenic Arc. We use a block modeling approach, as have previous studies [e.g., *Meijer and Wortel*, 1997; *Cianetti et al.*, 2001; *Kreemer and Chamot-Rooke*, 2004; *Reilinger et al.*, 2006]. The key advance represented by our model is incorporation of a detailed representation of the 3-D shape of the Nubian-Aegean plate contact. Other than paying careful attention to the subduction zone geometry, our model is a relatively simple set of elastic blocks. Nonetheless, we find that model results are consistent with the broadest features of the arc, such as topography and seismicity distribution. We derive the strain field of the overriding plate, the spatial distribution and orientation of differential stress ($\sigma_1 - \sigma_3$), and expected seismic moment release. We suggest that deformation is driven primarily by the fast moving Aegean upper plate overriding the relatively stagnant Nubian lower plate.

2. Model Development

[10] Our 3-D finite element model of the south Aegean region was built using the surficial plate boundary line as defined by *Kreemer and Chamot-Rooke* [2004]. We constrained slab geometry using deep earthquake locations [*Papazachos et al.*, 2000a; *Li et al.*, 2003; *Meier et al.*, 2004] and results from seismic profiling [*Bohnhoff et al.*, 2001]. We put in the level of detail that can be reasonably resolved with available observations, which resulted in a complex mesh (Figure 2). This involved identifying the plate interface by earthquakes, which are located within a few kilometers of vertical uncertainty. The slab was composed of two volumes: a 7 km thick oceanic crust [*Bohnhoff et al.*, 2001] and a 50 km thick mantle lithosphere [*Spakman et al.*, 1988]. The shape of the subducting Nubian plate resembles a funnel, or amphitheater (Figure 2) as the E-W dimension of the slab gets shorter and steeper with increasing depth, which is a necessary consequence of the shape of the Hellenic Arc. The slab is located at about 50 km beneath the island of Crete [*Meier et al.*, 2004] and 100 km beneath the island of Santorini [*Li et al.*, 2003]. We terminated the slab at 170 km depth in our model due to lack of seismicity below this level.

[11] We took particular care in developing the shape of the Nubian slab and its contact with the Aegean block, which has a difficult geometry to develop and mesh. However, the hypothesis we wanted to test was that the geometry of the slab and potentially dying subduction [e.g., *Le Pichon and Angelier*, 1981; *Wortel and Spakman*, 2000; *Faccenna et al.*, 2006; *Agostini et al.*, 2007] beneath the Hellenic Arc is important to regional deformation. We drew five cross section profiles of the interplate contact around the arc from well-located earthquake hypocenters [*Papazachos et al.*, 2000a; *Li et al.*, 2003; *Meier et al.*, 2004] and constrained the shallowest part of the contact from seismic profiling by *Bohnhoff et al.* [2001]. We generated the contact surface by skinning a surface through the specified guiding lines. The lines acted as a set of ribs over which a surface was "stretched" by a spline-fitting algorithm. Two opposite edges of the area were framed by the first and last guiding lines specified. The other two edges of the area were framed by spline fit lines generated through the ends of all guiding lines. An example along-dip profile describing the Nubian slab is given in Table 1.

[12] The Aegean upper plate volume was constructed from three layers: a 15 km thick upper crust, a 15 km thick lower crust, and a 50 km thick mantle lithosphere. This representation of the lithosphere is more accurate toward the south and east parts of the arc than to the west and north, where thickened (40 + km) continental crust still persists beneath central Peloponnese [*van der Meijde et al.*, 2003; *Sachpazi et al.*, 2007]. For example, beneath the island of

Table 1. Variation in the Dip of the Modeled Nubian Slab Along a Sample (Easternmost Edge) Cross Section[a]

Depth (km)	Subduction Angle (deg)
0	9
−1	9
−2	9
−3	9
−3	9
−4	9
−5	8
−6	9
−9	11
−10	16
−13	20
−15	24
−22	30
−25	36
−30	39
−43	43
−48	46
−53	47
−58	48
−69	50
−74	51
−80	51
−85	52
−91	52
−96	53
−102	53
−113	53
−124	53
−130	54
−135	54
−141	54
−158	55
−164	55
−170	56

[a]The slab angle increases with depth (Figure 2).

Gavdos the continental Moho is located at −26 km [*Li et al.*, 2003]. No topography or bathymetry was included in the model, which had an initial flat surface located at sea level. All model coordinates were in km on a Mercator projection centered at 25°E, 37°N. Boundary condition regions of the model extend far from the subduction zone so that their effects are minimized.

[13] The upper crust of the Aegean block was assumed to have granitic material properties, the lower crust was associated with basaltic properties, and the upper mantle was defined by dunite. The Nubian slab upper crust was assumed to be basaltic, while the slab mantle lithosphere was assumed to have the same elastic properties as the Aegean upper mantle. Material constants are listed in Table 2.

[14] Volumes were meshed by first estimating element edge lengths for all defining lines. The element edge lengths on these lines were then refined for curvature and proximity of features in the geometry. The mesh was thus finest where volumes changed shape the most, and in regions of greatest complexity. Since the mesh was scaled by line lengths, elements in the thinnest parts of the crustal layers were much smaller than in the thickest parts (Figure 2). A variable-sized mesh approach reduced the number of nodes in parts of the volumes where they were not needed, making the model more computationally efficient without sacrificing accuracy. The model was composed of 73,133 elastic tetrahedral elements defined by 106,962 nodes with an average node spacing of 25 km. Elements were defined by 10 nodes, each having 3 degrees of freedom (translations in the nodal x, y, and z directions).

[15] Our Aegean finite element model had one major contact zone, representing subduction of the Nubian plate beneath the Aegean (Figure 2). This fault was deformable, and was constructed from contact elements obeying the Coulomb failure (CF) relation

$$\mathrm{CF} \equiv \tau_f + \mu(\sigma_n) \tag{1}$$

where τ_f is shear stress acting on a fault surface, μ is the friction coefficient, and σ_n is the component of stress acting normal to a fault surface. Contact elements had zero thickness and were welded to the sides of tetrahedral elements. We assigned a low friction coefficient ($\mu = 0.2$) to the subduction interface [e.g., *Cattin et al.*, 1997; *Ruff*, 2002; *Kopf and Brown*, 2003; *Ring and Reischmann*, 2002], although this parameter is not important in a steady state model.

[16] Our modeling focus was limited primarily to Nubian and Aegean block interaction across the subduction front. We thus did not include the north Anatolian fault, which is the strike-slip boundary between the north Aegean and Eurasia, or other transtensional structures of the north Aegean [*Taymaz et al.*, 1991; *Ganas et al.*, 2005] or west Anatolia [*Aktar et al.*, 2007; *Papanikolaou and Royden*, 2007]. Since we used observed GPS vectors to displace the model blocks (Figure 1), any remote contribution from distant faults like the north Anatolian is accounted for, although given the uniformity of velocity observations in the south Aegean, there is little indication of such contributions. We loaded our model by applying displacements to its edges. We relied on summaries of major block motions developed from GPS observations [*Nyst and Thatcher*, 2004; *Reilinger et al.*, 2006]. The southern model block represented the Nubian plate, and was moved at a 5 mm a^{-1} rate on a N10°W vector relative to stable Eurasia (Figure 2). The northern model block represented Aegean lithosphere, which was moved along a N215°E direction at a 33 mm a^{-1} rate. These combined motions resulted in a ∼35–40 mm a^{-1} convergence rate depending on the plate boundary orientation. The Aegean block was constrained not to sink along its base, but could slip freely, simulating the asthenosphere-lithosphere boundary. The Nubian plate was constrained to stay within the subduction channel, but was allowed to descend freely. Thus the subduction hinge was not allowed

Table 2. Material Constants Used in the Three Layers of the Finite Element Model[a]

Parameter	Upper Crust Layer	Lower Crust Layer	Upper Mantle
E, Young's modulus (MPa)	8×10^4	9×10^4	1.9×10^5
ν, Poisson's ratio	0.25	0.26	0.28
ρ, density (kg m^{-3})	2.7×10^3	2.8×10^3	3.0×10^3

[a]Elements in the model were elastic. Data from *Birch* [1966], *Christensen* [1996], *Christensen and Mooney* [1995].

to roll back. We discuss the implications of these boundary conditions in section 3.

3. Effects of Model Assumptions and Data Limitations

[17] Results presented here depend on the quality of the input data and many assumptions inherent in projecting information measured at the surface to great depth. The surface trace of the Hellenic Arc was projected through the model based primarily on the positions of well-located earthquakes. However, we did make a major assumption that these events represent the interplate contact. Thus our model is sensitive to earthquake location errors and possible misassignment of earthquakes to the subduction interface. Further, while the funnel, or amphitheatrical shape of the descending slab in our model is likely correct to first order [e.g., *Papazachos et al.*, 1995, 2000a; *Faccenna et al.*, 2006; *Husson*, 2006; *Snopek et al.*, 2007], the shape of this surface represents an interpolation between constrained profiles. A smoothed simplification of the actual shape likely produced more smoothly varying deformation results than what happens in the real Earth.

[18] A major limitation in our model is the fact that we did not allow the Nubian-Aegean subduction hinge to roll back to the south. This process is a common attribute in many tectonic models in the region [e.g., *Le Pichon and Angelier*, 1981; *Wortel and Spakman*, 2000; *Reilinger et al.*, 2006; *Faccenna et al.*, 2006]. We did not allow this to occur in the 3-D model because of the significant complexities introduced by its inclusion, such as requirements for (1) asthenosphere outflow behind the hinge, (2) appropriate fractured rheology for the bending part of the slab, and (3) inclusion of continental Africa, which would act to resist rollback. We concluded that modeling these processes might introduce more uncertainty than constraints. We further note that GPS observations, while few on the Nubian plate (Figure 1), show northwest motion relative to Eurasia within 50–100 km of the subduction front, leaving little space for any rollback. This scientific process allows us to clearly state the model dynamics that we are testing and compare them against the existing observations (uplift, moment rates and strain patterns). If we can fit those to first order, we do not see cause for incorporating unconstrainable complexity. In section 4 we show that our simplified approach, in combination with observed deformation patterns, enabled us to broadly quantify the relative role that subduction hinge rollback plays in the south Aegean.

[19] A relatively dense array of GPS observations is available for the Aegean and surrounding regions [*Nyst and Thatcher*, 2004; *Reilinger et al.*, 2006; *Hollenstein et al.*, 2008]. In our model we used average velocity vectors for displacement loads on the major blocks because these blocks were not broken by faults. The GPS data span a period of 20+ years from a spatially distributed network of 558 bench marks (Figure 1) that constrain the deformation of the westernmost part of Anatolia and most rapidly deforming part of the south Aegean and central Greece. Therefore variations in predicted patterns of interplate slip (and hence seismic moment) result only from geometric considerations, and omit any variability that might occur from subblock-scale relative motions. In summary, an attempt was made to include as much detailed information on crustal structure and deformation rates as possible, but calculated deformation results should be interpreted with the caveat of considerable uncertainty.

4. Model Results and Discussion

4.1. Predicted Versus Observed Uplift

[20] One of the enigmatic features of island arcs is the elevated strip of crust that emerges before the advancing oceanic lithosphere. For the Hellenic Arc, the models that have been proposed so far include (1) sediment accumulation scraped off of the subduction interface [e.g., *Le Pichon and Angelier*, 1981; *Le Pichon*, 1983; *Taymaz et al.*, 1990], (2) lithospheric flexure [*Giunchi et al.*, 1996], (3) mass deficit beneath western Crete [*Snopek et al.*, 2007], and (4) extrusion of lithospheric material of the Aegean plate [*Meier et al.*, 2007]. Our finite element model did not provide opportunities to test these ideas because it lacked sediment that could be detached from the downgoing slab, and it had no asthenosphere above which flexure, or isostacy-driven elevation changes could occur. Instead our model focused on deformation implications of the interplate contact shape. As discussed below though, we found that the expected spatial distribution of relative uplift from our finite element model is very consistent with observations, and that much of it can be explained from geometrical considerations.

[21] The finite element model predicted radial deformation and uplift of the upper plate as a result of it being pushed up the Nubian slab. We briefly discuss the origins of the interplate contact shape here. The Nubian slab is nearly passive as compared with the Aegean block, which overrides it at a velocity more than 6 times faster. Nubian plate subduction geometry is likely a function of slab age, slab detachment at ~200 km depth, and deformation of the slab due to continental collision to the east [e.g., *Le Pichon and Angelier*, 1981; *Spakman et al.*, 1988; *Wortel and Spakman*, 2000; *Kreemer and Chamot-Rooke*, 2004; *Reilinger et al.*, 2006; *Faccenna et al.*, 2006]. The funnel or amphitheatrical shape of the Nubian slab may have been created after slab detachment that accelerated trench rollback, which in turn may have tightened the Hellenic Arc radius [*Regard et al.*, 2005; *Faccenna et al.*, 2006; *Husson*, 2006]. We speculate that these forces bent a weakened Nubian slab into its current configuration. The progressive deformation of the downgoing slab is evidenced by the focal mechanisms of intermediate depth earthquakes that indicate E-W compression [*Benetatos et al.*, 2004].

[22] In this setting of active convergence, our model suggests that uplift results from the fast moving overriding Aegean block is being pushed up the plate interface; the model indicates maximum uplift where the subduction angle decreases between 20 and 50 km depths (Figures 2 and 3). We predict the greatest amplitude of uplift centered at the island of Crete; the effect tapers off into the adjacent regions such as the south Peloponnese to the west, and the island of Rhodes to the east (Figure 3). Published geological observations are consistent with our simulations (Figure 3) [*Flemming*, 1978; *Le Pichon and Angelier*, 1981; *Pirazzoli et al.*, 1982, 1989, 1996; *Meulenkamp et al.*, 1994; *Price et*

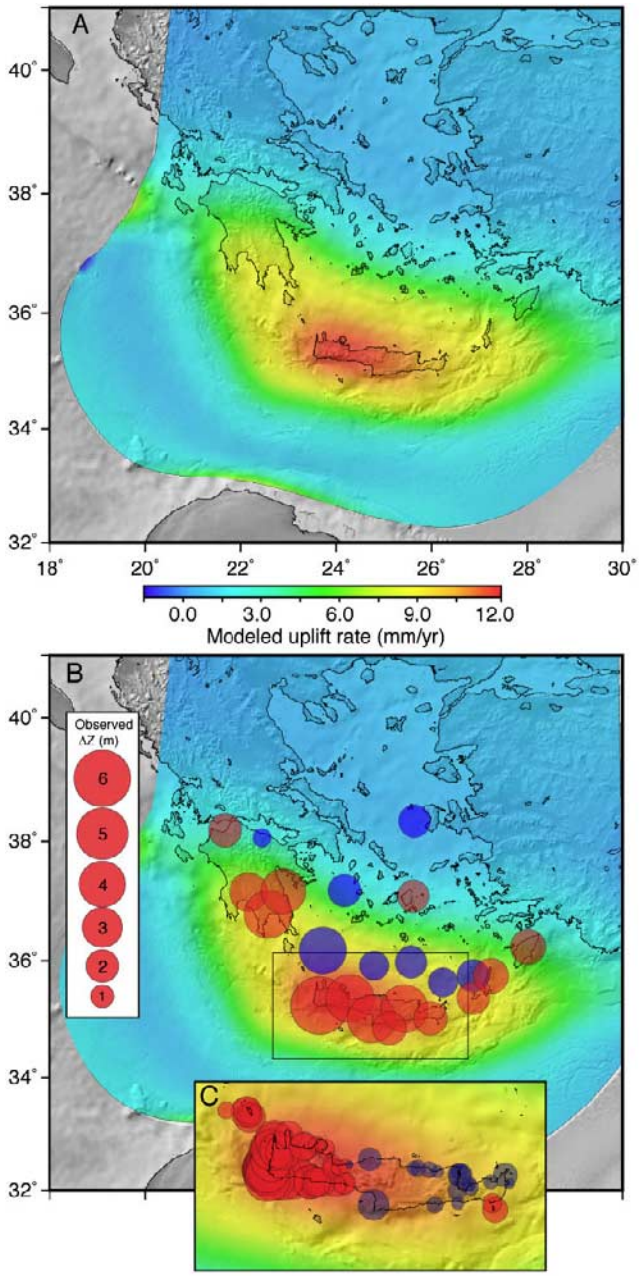

Figure 3. (a) Map of modeled uplift rate (mm a^{-1}) along the Hellenic Arc. (b) Observed values of uplift. Box shows expanded area of Crete in Figure 3c. Solid circles indicate localities of geological data reported by *Flemming* [1978], *Le Pichon and Angelier* [1981], *Pirazzoli et al.* [1982, 1996], and *Price et al.* [2002]. Circles are shown proportional to observed values on top of shaded contouring which is model. Red is uplift and blue indicates subsidence, respectively. (c) Expanded area of Crete.

al., 2002]. The locus of greatest observed uplift rates is central and western Crete, which is about halfway around the arc. Furthermore, uplifted Holocene coastlines have been mapped inside the back-arc region as far as Samos island [*Stiros et al.*, 2000], and the Corinth rift in central Greece [*Houghton et al.*, 2003; *De Martini et al.*, 2004; *Pirazzoli et al.*, 2004; *Kershaw et al.*, 2005]. Previous 2-D, numerical modeling work by *Giunchi et al.* [1996] was able to match geological data along the south coast of Crete but not along the north and west coasts of the island.

[23] Although we predict tectonic uplift in these regions (Figure 3), not all observed uplift results from plate convergence because there is well-established evidence for coseismic uplift inside rift systems [e.g., *Jackson et al.*, 1982; *Stein et al.*, 1988; *Meyer et al.*, 1996; *Meghraoui et al.*, 2001]. Our model did not reproduce observed subsidence in the south Aegean Sea north of Crete, likely a result of the model upper plate being unbroken by faults.

[24] To summarize, our 3-D finite element model calculates a spatial distribution of uplift broadly commensurate with observations along the Hellenic Arc and within an order of magnitude (given the measurement uncertainties). The finite element model can reasonably match the relative uplift patterns with just a 3-D representation of the interplate contact and no crustal faults. However, calculated uplift amplitudes exceed geological measurements (mean Holocene uplift rates; see *Pirazzoli et al.* [1996] and *Price et al.* [2002] for a summary) by about 3–6 mm a^{-1}, or nearly double. There are at least three factors contributing to this: (1) no erosion was allowed in the model, (2) no isostatic balance was included, and (3) no subduction rollback was allowed. If we had a way of accurately incorporating these effects, they would reduce the amount of calculated uplift.

[25] As a test of our conclusions about Cretan uplift, we investigated the hypothesis that it is due to repeated, coseismic displacements [e.g., *Pirazzoli et al.*, 1996; *Stiros*, 2001; *Shaw et al.*, 2008; *Papadimitriou and Karakostas*, 2008]. We model coseismic uplift at 0 (sea) level due to seismic motion along the interplate contact beneath Crete. We used a dislocation model derived from recent data on the depth and the dipping angle of the interface beneath Crete [*Bohnhoff et al.*, 2001; *Meier et al.*, 2004, 2007]. Displacement is due to simple, planar slip along the source fault in an elastic half-space [*Okada*, 1992] by assuming a shear modulus of 3.0×10^{11} dyn cm^{-2} and Poissons ratio 0.25. The modeling parameters are summarized in Table 3. We used the code DLC written by R. Simpson (USGS) to simulate coseismic displacements on an elastic Earth. We introduced an earthquake of Mw = 8.2 (maximum expected according to *Hamouda* [2006]) on a thrust fault with length of 160 km and rupture width of 50 km (based on the seismogenic interface estimates of *Laigle et al.* [2004]). The epicenter was assumed at 35.3°N and 23.5°E, right offshore the southwest corner of the island (approximately 3 km to the west of the Chrisoskalitissa monastery; circle in Figure 4a). The depth of the hypocenter was 50 km as the interplate contact is estimated to be at a depth of about 40–55 km beneath Crete [*Meier et al.*, 2007]. We believe that there is no other fault plane offered for a Mw = 8.2 rupture at shallower depths (like the model of *Shaw et al.* [2008]) as there is no evidence for microseismity beneath western Crete at depths >20 km and <40 km [see *Meier et al.*, 2007, and references therein].

[26] We model the hypocenter at the center of the rupture plane (see Figure 4a inset for a cross section view) and assumed uniform slip. This is an obvious simplification of the dislocation model as subduction-type "megaevents"

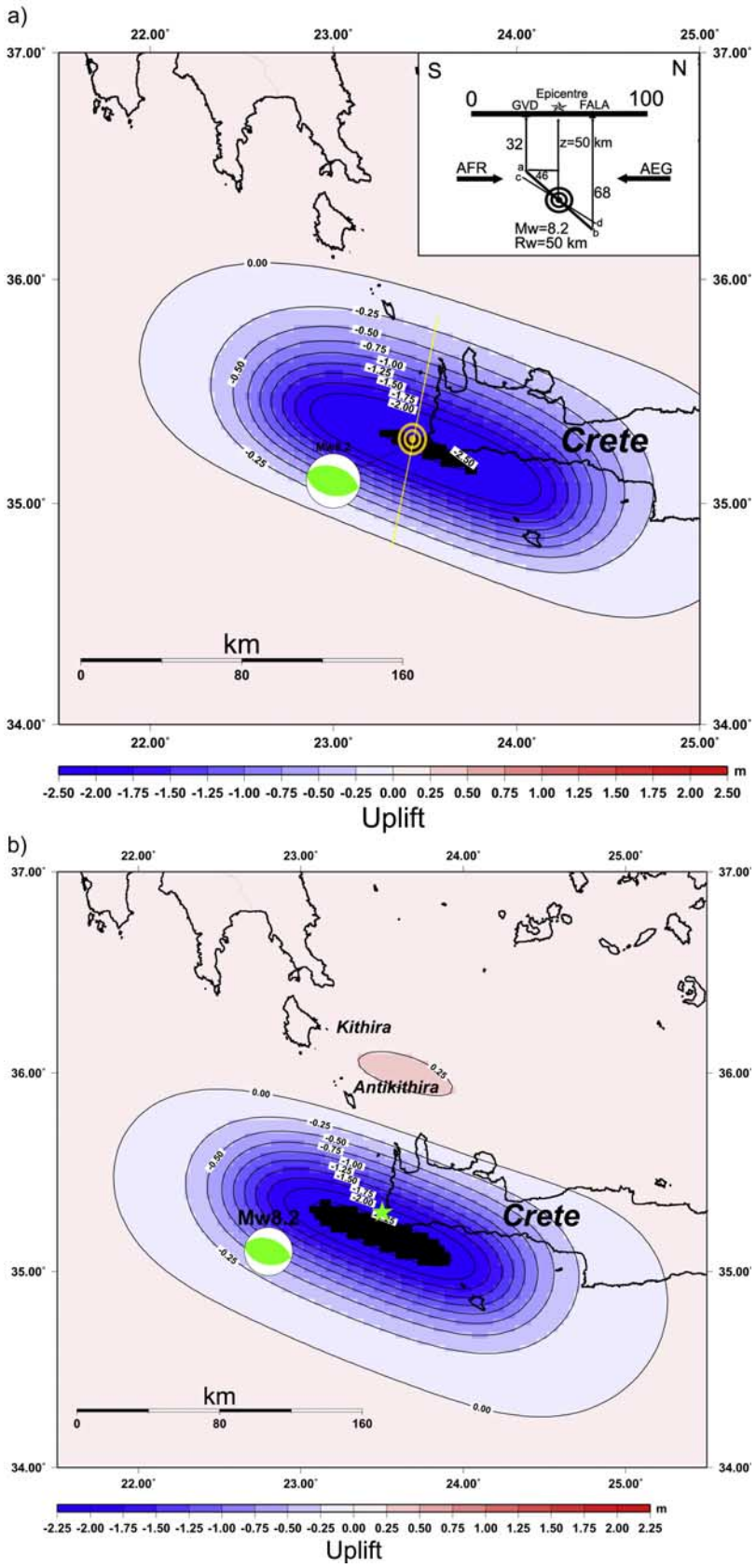
a)
22.00°
23.00°
24.00°
25.00°
37.00°
36.00°
35.00°
34.00°
S
N
0
Epicentre
GVD
FALA
100
32
z=50 km
AFR
AEG
46
68
Mw=8.2
Rw=50 km
Crete
Mw8.2
km
0
80
160
m
-2.50 -2.00 -1.75 -1.50 -1.25 -1.00 -0.75 -0.50 -0.25 0.00 0.25 0.50 0.75 1.00 1.25 1.50 1.75 2.00 2.50
Uplift
b)
Kithira
Antikithira
Crete
Mw8.2
km
0
80
160
m
-2.25 -2.00 -1.75 -1.50 -1.25 -1.00 -0.75 -0.50 -0.25 0.00 0.25 0.50 0.75 1.00 1.25 1.50 1.75 2.00 2.25
Uplift

Figure 4

Table 3. Modeling Parameters Used to Calculate Coseismic Uplift of Crete

Parameter	Value
Poisson ratio	0.25
Shear modulus	3×10^{11} dyn cm^{-2}
Map projection	UTM zone 34
Depth of hypocenter	50 km
Displacement grid size	1 km
Length/width of rupture	160/50 km
Fault plane (dextral)	N290°E/46°NE and 36°NE/97° (strike/dip/rake)

show nonuniform and asymmetric slip distribution along strike of the plate boundary [e.g., *Vigny et al.*, 2005; *Subarya et al.*, 2006]. Despite this fact we still think it is worthy to get the simplified deformation field given the best possible constraints we can incorporate from the literature for this part of the world. The modeled rupture stops at a depth of 68 km in accordance with focal mechanism data from intermediate depth earthquakes along the Hellenic Arc [*Benetatos et al.*, 2004] which indicate a drastic change in the stress field from arc-normal to arc-parallel compression at depths 50–60 km. The resulting moment "of this mega-event" was 2.04×10^{28} dyn cm. Slip at the hypocenter equaled 8.25 m of updip and 1.01 m of right-lateral motion as we allowed for a small dextral component of the slip vector in accordance with the GPS data [*Hollenstein et al.*, 2008] and the findings of our modeling (see Figure 6). Such modeled coseismic slip amounts are in agreement with results from space geodesy of [$8 < M < 8.3$] plate boundary events in Mexico [*Hutton et al.*, 2001] and Chile [*Chlieh et al.*, 2004]. Moreover, our modeled rupture stops at a depth of about 32 km roughly beneath the island of Gavdos (see Figure 4a inset) so it is not expected to reach the sea bottom and cause a tsunami such as the one that was observed in 365 A.D. [*Pirazzoli et al.*, 1996; *Stiros*, 2001].

[27] The surface displacement maps are shown in Figure 4 for two cases of the north dipping interface, which is with a dip angle of 46° to the NE (Figure 4a and Table 1) and with a dip angle of 36° according to the estimates of *Papazachos et al.* [2000a] (Figure 4b and Figure 4a inset). The maps also show contours of isodisplacement (surface uplift) at 0.25 m intervals. The resulting surface uplift is between 2.5 and 2 m for the southwestern corner of Crete, decreasing to the north and east. The island of Antikithira where uplifted coastlines have been mapped by *Pirazzoli et al.* [1982] is uplifted around 25 cm (maximum). No uplift is predicted farther north (Kithira Island) or eastern Crete where geological evidence suggests uplift [e.g., *Fortuin*, 1978].

[28] Another weakness of DLC-type, planar dislocation models to match the geological data on uplift above subduction zones results from dislocation models having symmetric slip, with the upper plate getting 50% of the motion, while the lower plate moves down with the other 50%. In our 3-D FEM (Figure 2), we model the upper plate riding up the slab, which is nearly fixed. Our uplift pattern (Figure 3) thus results from the asymmetric relative rate of the two blocks. We suggest that ~2-D symmetric slip models are inadequate for modeling displacements close to plate boundaries because they cannot accommodate features like lithosphere-scale relative block motion.

[29] To put more emphasis on the failure of coseismic models to explain the geological data for uplift, we consider the cumulative deformation over the last 1650 years (since 365 A.D.) neglecting the postseismic component. We assume that tectonic uplift rates continue to accumulate today as during the Holocene period. The geological uplift rates in SW Crete average 3 mm a^{-1} (maximum 5–6 mm a^{-1}; site Chrisoskalitissa [*Pirazzoli et al.*, 1996; *Price et al.*, 2002]) or 5 (maximum 8) m in 1650 years, in other words the cumulative coseismic uplift (since 365 A.D.) should equal this geological uplift. However, adopting a slip model like the one presented in Figure 4 (resulting in 2.2–2.5 m of coseismic uplift) we need to invoke two (2) to four (4) such events (excluding 365 A.D.) in order to accumulate 5 m (maximum 8 m) of uplift with a return period of nearly 800 (400) years. Clearly the historical data [*Papazachos et al.*, 2000b] do not show any evidence to support this hypothesis. Such short average return periods are consistent with no historical record of prior M = 8 events in the eastern Mediterranean. We suggest that (1) the maximum uplift of SW Crete due to a M = 8.2 earthquake along the plate interface does not exceed 2.5 m, (2) this coseismic uplift can explain neither the pattern of uplift provided by the geological data nor the ground data (amount of uplift in Figure 3), and (3) this coseismic uplift fails to match the historical record (last 1650 years) as too short return periods are necessary. We conclude that our 3-D deformation model explains the origin of the uplift better than coseismic uplift due to "megaevents" along the Hellenic Arc.

4.2. Predicted Versus Observed Moment Rate Distribution

[30] Our model of Aegean-Nubian plate interaction enabled calculation of expected slip rate (u) on the interplate

Figure 4. (a) Map of coseismic uplift estimates for a 46° dipping interface between Aegean and Nubia (Africa) plates. Sign convention is minus for uplift and plus for subsidence. Calculations are shown for displacements at sea level. Areas shown in black denote up to 5 cm of offshore uplift greater than the maximum contoured uplift. Beachball indicates modeled focal mechanism of the earthquake (lower hemisphere equal-area projection, green is compression). Inset features include the following: a thick horizontal line is sea level, star is epicenter of Mw = 8.2 event, thick inclined line constrained by small letters a and b is rupture plane along plate interface dipping at 46°, concentric circles are hypocenter at 50 km depth, 32 is depth of point (number) a, 68 is depth of point (number) b, thin inclined line constrained by small letters c and d is rupture plane along plate interface dipping at 36°, Rw is width of rupture plane (50 km), GVD is island of Gavdos (see Figure 1 for a map view), FALA is uplifted ancient port of Falassarna, arrow with AFR denotes Africa (Nubia) plate motion, arrow with AEG is Aegean plate motion. (b) Map of coseismic uplift estimates for a 36° dipping interface between Aegean and Nubia (Africa) plates. Symbols, labels, and signs are as in Figure 4a.

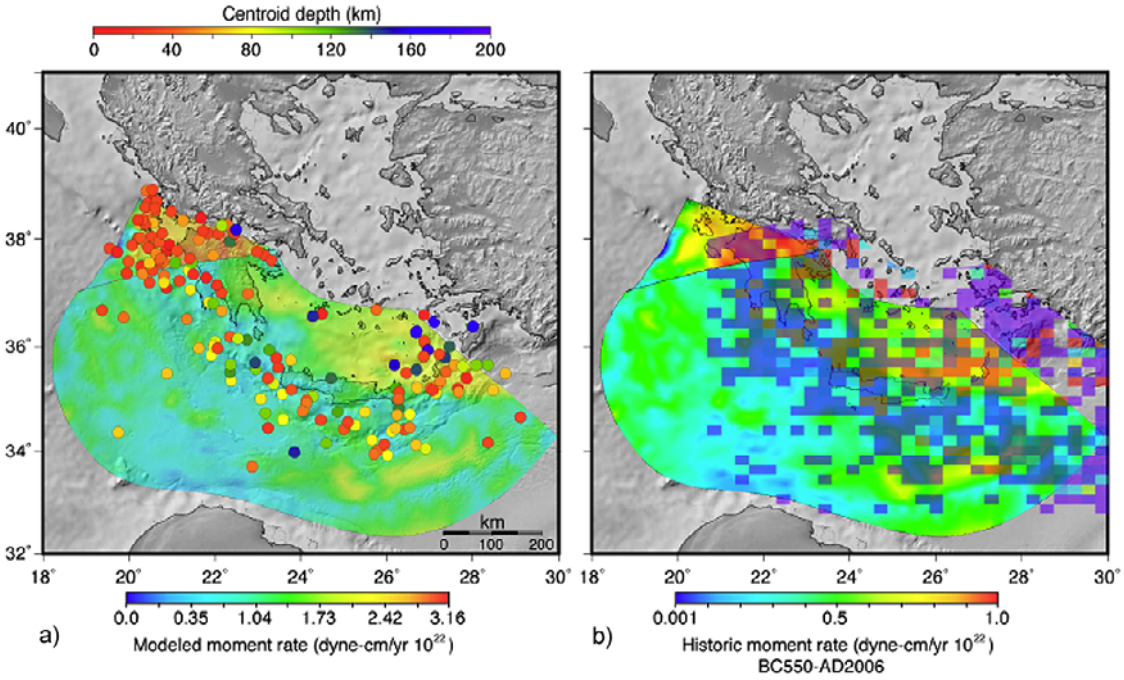

Figure 5. Comparisons between calculated expected seismic moment rate distribution from the finite element model, and observed instrumental event locations (a) from the Harvard CMT catalog and (b) with the 550 B.C. to 2006 A.D. historical catalog [*Papazachos et al.*, 2000b]. Harvard CMT epicenters are shaded by depth. The historical catalog was gridded into 0.1° cells, magnitudes converted to moment, and moment rates were calculated for each cell.

megathrust, which was used to calculate the expected seismic moment rate (M) distribution as

$$M = \mu A u, \tag{2}$$

where A is fault area and μ is the shear modulus (where $\mu = 3 \times 10^{11}$ dyn cm^{-2}; Figure 5).

[31] The model calculations show more detail in expected moment rate distribution than is likely warranted, given the coarse scale of the input data on slab geometry (Figure 5). However, the broader-scale pattern shows trends that are interpretable. Model calculations suggest a generally higher seismic moment release on the eastern side of the megathrust and to the northwest near the Cephalonia transform (Figure 5), where calculated moment release is nearly double that in the west central part. Below we compare the calculated cumulative moment release with observed, as well as differences and similarities between spatial moment release distributions.

[32] We tested our expected cumulative annual moment rate map against the records of the Global CMT database (http://www.globalcmt.org) and the catalog of *Papazachos et al.* [2000b] (updated regularly), which spans the period 550 B.C. to 2006 A.D. (Figure 5). From our model we calculate a cumulative seismic moment rate of 3.38×10^{25} dyn cm a^{-1} across the interplate contact area shown in Figure 5, which extends from the surface to a 170 km depth. We summed 31 years of the regional Harvard CMT catalog and found an observed cumulative seismic moment rate of 6.98×10^{25} dyn cm a^{-1} for all regional earthquakes (Figure 5). If we restricted the summation to thrust events (rake range −135° to 135°, which we assume absorb Aegean-Nubian convergence whether they occur on the megathrust or on other structures), we found that the CMT catalog moment release was 3.78 10^{25} dyn cm a^{-1}. Thus the model cumulative convergent moment rate agrees within 10% of the observed rate. Summing the 550 B.C. to 2006 A.D. catalog (Figure 5b), we found an expected cumulative annual moment rate of 5.79×10^{22} dyn cm a^{-1}, considerably less than either the CMT catalog or the model rate. This is likely a result of the historic catalog being incomplete.

[33] We acknowledge considerable uncertainty in observed versus calculated seismic moment rate comparisons, but the results are suggestive of a high-to-complete coupling coefficient beneath the Hellenic Arc, an unusual result compared with other subduction zones [*Bird and Kagan*, 2004]. A speculative explanation is that if the deep Nubian slab (>200 km depth) was removed as many investigators have suggested [e.g., *Spakman et al.*, 1988; *Wortel and Spakman*, 2000; *Faccenna et al.*, 2006], then there may be a smaller slab-pull force than in most subduction zones. The lack of slab pull means potentially less reduction in the normal stress across the interplate contact [e.g., *Brune and Thatcher*, 2002] and increased seismic coupling. Further, if our model is correct, then the Aegean block is colliding with, and overrunning an essentially stalled Nubian plate. This setting may thus have more in common with continental thrust zones than classic subduction zones [*Bird and Kagan*, 2004], hence the higher coupling.

[34] The spatial pattern of calculated moment release suggests higher seismic moment release on the eastern side of the Hellenic Arc, and also beneath the most northwest-

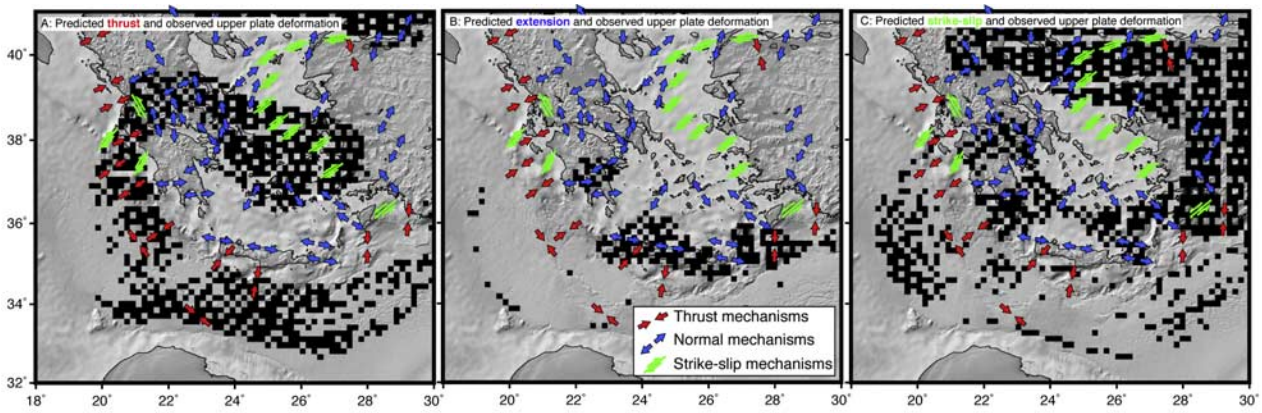

Figure 6. Comparison of modeled tectonic regime and observed upper plate deformation as provided by seismicity [*Kiratzi and Louvari*, 2003]. Black squares are modeled deformation depending on the orientation and magnitude of principal stresses. Double arrows indicate type of focal mechanism as follows: (a) red is reverse faulting, (b) blue is normal faulting, and (c) green is strike-slip faulting. Modeled deformation is in reasonable agreement except for the region of central Greece (Figure 6a) where extension prevails. Thus, much of the Aegean block strain might be attributed to its interaction with the Nubian plate.

erly part, adjacent to the Cephalonia transform (Figure 5). Both observed catalogs show mildly higher moment release on the eastern side of the Hellenic Arc and near the Cephalonia transform, broadly matching the expected pattern from the modeled moment rate. Additionally, model calculations showed a 400 km long zone of higher expected seismic moment rate located south-southeast of Crete; no global CMT events have occurred in this zone (Figure 5), but the historic catalog of *Papazachos et al.* [2000b] suggests some moment release there. Thus this area could represent a seismic gap. A similar mismatch between the model and observed moment release is seen north of Crete, where the calculated spatial pattern is only similar to the longer *Papazachos et al.* [2000b] catalog. Furthermore, our calculated moment rate map that shows no focused high slip beneath Crete (therefore, there is no need for $M > 8$ events) while at the same time, the Cretan uplift is focused there by 3-D geometric effects of the funnel-shaped slab. An implication of this result is that tsunami-related studies in this region [e.g., *Yolsal et al.*, 2007; *Lorito et al.*, 2008; *Shaw et al.*, 2008] may consider alternative fault sources such as the area of the plate interface about 150 km to the west-southwest of Peloponnese and 150 km to the south of Crete (Figure 5) where predicted seismic moment rate is the highest on the convex side of the Hellenic Arc.

[35] To summarize, we found that our model of a fully coupled Aegean-Nubian plate contact can only account for ~90% of the observed CMT catalog thrusting in the region. This is an unusual result for a subduction zone, where expected moment release usually exceeds observed because of low coupling [*Bird and Kagan*, 2004]. We suggest that the Hellenic Arc is more fully coupled because the nearly stalled Nubian slab is being overridden by a fast moving Aegean block. We calculated that the observed bias of more seismic moment release on the east side of the Hellenic Arc and near the Cephalonia transform can be explained by the shape of the interplate contact and the relative plate motion vector.

4.3. Predicted Versus Observed Strain Mode Distribution

[36] We thought it would be interesting to see how our simple model of Aegean block (upper plate) deformation compared with observed regional strain patterns. Since all deformation in our model was produced by interaction between the Nubian and Aegean blocks, the comparison allowed us to assess the role of the plate boundary geometry. Our upper plate model was unbroken by faults, so our basis for comparison was variation in the modeled stress tensor versus patterns of dominant earthquake mechanisms. In particular, the strain analysis is limited to effects of Nubian-Aegean interactions and our model lacks interactions between Eurasia and the Aegean block. Since we are modeling just the subduction zone effects, we do not presume to have solved for all the strain in the Aegean. Rather, our results posit what the isolated components of strain are from interactions between Nubia and Aegean block, and we suggest that mismatches likely result from Eurasian-Aegean interactions to the north.

[37] We resolved the stress tensor into principal stresses at each model node. Expected thrust, strike-slip, and normal fault regimes were classified according to greatest and least principal stress orientations [*Anderson*, 1951]; for example if the greatest principal stress was within 30° of vertical while the least principal stress was within 30° of horizontal, we classified the stress state as extensional. The same criteria were applied in defining thrust and strike-slip regimes. The defined stress regimes were compared with a summary of spatial distribution of earthquake mechanisms [*Kiratzi and Louvari*, 2003] (Figure 6; see also focal mechanisms on Figure 1).

[38] As might be expected given the focus of our model, we found best agreement between calculated stress orientations and observed strain patterns nearest to the Hellenic Arc (Figure 6). Modeled stresses showed that thrusting is expected to be distributed around the surface trace of the Nubian plate subduction, which is in agreement with

observed (Figure 6a). The 14 February 2008 thrust event (Mw = 6.7; http://earthquake.usgs.gov/eqcenter/eqinthenews/2008/us2008nkan/) confirmed our predictions as it occurred 30 to 40 km offshore the SW Peloponnese. However, the model predicts thrusting in the central Aegean Sea, whereas the observed strain pattern is mostly strike slip [*Taymaz et al.*, 1991].

[39] Our model captured some observed extensional deformation, primarily around the island of Crete and in the southern Peloponnese (Figure 6b) where onshore geological data suggest crustal extension [*Armijo et al.*, 1991, 1992; *Roberts and Ganas*, 2000; *Caputo et al.*, 2006]. *Mascle and Martin* [1990] presented many fault scarps inside the central and eastern Cretan Sea (south Aegean) where our model predicted extension and strike-slip deformation. The model did not reproduce observed extension north of the Peloponnese [e.g., *Jackson et al.*, 1982; *Papazachos et al.*, 1983; *Roberts and Ganas*, 2000; *Meyer et al.*, 1996], nor in the north Aegean [e.g., *Brooks and Ferentinos*, 1980; *Pavlides and Tranos*, 1991], or Anatolian block, which likely has different origins than that from around Crete. The extension in our model resulted from uplift (Figure 3) and resulting subsequent spreading.

[40] Our model did not match observed strike-slip deformation very well, missing most of the south central Aegean observations (Figure 6c) [*Benetatos et al.*, 2006; *Aktar et al.*, 2007] but fitting the north central Aegean data [e.g., *Kiratzi et al.*, 1991; *Pavlides and Tranos*, 1991; *Taymaz et al.*, 1991; *Ganas et al.*, 2005]. The model also predicted strike-slip strain patterns in NW Peloponnese (Figure 6c) where the 8 June 2008, 1225:30 UTC, Mw = 6.4, right-lateral and shallow event took place (http://earthquake.usgs.gov/eqcenter/eqinthenews/2008/us2008taaw/) [*Ganas et al.*, 2009]. There was some expectation in the model of broadly distributed strike-slip strain in the Anatolian block where the right-lateral north Anatolian fault occurs.

[41] To summarize, we found a surprising variation in expected crustal strain in the Aegean upper plate given the primarily convergent nature of Aegean-Nubian plate interaction. We attribute the variable strain mode distribution (as inferred from the stress tensor) to the slightly oblique convergence and the unusual funnel, or amphitheatrical shaped Nubian plate.

5. Conclusions

[42] In assembling a kinematic model of Hellenic Arc subduction, we noted some unique features: (1) The Nubian slab has a funnel, or amphitheatrical shape, and is likely detached or torn at about 200 km depth. (2) The Aegean (upper plate) block moves much faster to the south ($\sim$33 mm a^{-1} relative to stable Eurasia) than the Nubian plate moves northward ($\sim$5 mm a^{-1}). (3) Deformation behind the arc combines regions of concentrated rapid (up to 6 mm a^{-1}) uplift, and a mixture of contractional, extensional, and transform strain.

[43] We developed a simple 3-D model that concentrated on the shape of the interplate contact (Figure 2). However, when we displaced model blocks according to their GPS-constrained velocities, we found that we could explain the uplift pattern and distribution of upper plate strain near the Hellenic Arc. M > 8 earthquakes along the plate interface cannot uplift the island of Crete for more than 2.5 m per event so our results do not support a 365 A.D. scenario for uplift. Further, when we compared the expected sum and distribution of expected seismic moment release related to Aegean-Nubian convergence, we found that the predicted moment release was within 90% of observed. We concluded that the Hellenic Arc was thus more completely coupled than typical subduction zones.

[44] Our interpretation of the Hellenic Arc is that it behaves more like a continental thrust belt because (1) it appears that the fast moving Aegean block overrides an almost stalled Nubian plate, (2) the resulting collision causes very high seismic activity rates and nearly complete seismic coupling, and (3) as the Aegean block rides up the Nubian slab, it is permanently uplifted as exemplified by formation of the island of Crete, which continues to rise at $\sim$6 mm a^{-1} rates.

[45] **Acknowledgments.** We thank the Fulbright Foundation for funding A.G.'s visit to USGS where this paper was written. Aspects of this research were funded by the Greek Secretariat for Research and Technology (GSRT). We thank Bob Simpson for providing his DLC code. Background topography was extracted from the SRTM30PLUS shaded relief data set [*Poppe et al.*, 2005]. Figure 4 was done by use of GMT software. We thank reviewers Tuncay Taymaz and Dimitri Papanikolaou for comments and suggestions. Nikolitsa Alexandropoulou helped compiling the geological data on Cretan uplift.

References

Agostini, S., C. Doglioni, F. Innocenti, P. Manetti, S. Tonarini, and M. Y. Savasçin (2007), The transition from subduction-related to intraplate Neogene magmatism in the western Anatolia and Aegean area, in *Cenozoic Volcanism in the Mediterranean Area*, edited by L. Beccaluva, G. Bianchini, and M. Wilson, *Spec. Pap. Geol. Soc. Am.*, *418*, 1–15, doi:10.1130/2007.2418(01).

Aktar, M., H. Karabulut, S. Ozalaybey, and D. Childs (2007), A conjugate strike-slip fault system within the extensional tectonics of western Turkey, *Geophys. J. Int.*, *171*(3), 1363–1375, doi:10.1111/j.1365-246X.2007.03598.x.

Ambraseys, N. N. (2001), Far-field effects of eastern Mediterranean earthquakes in lower Egypt, *J. Seismol.*, *5*, 263–268, doi:10.1023/A:1011476718680.

Anderson, E. M. (1951), *The Dynamics of Faulting and Dyke Formation*, 206 pp., Oliver and Boyd, Edinburgh, U. K.

Anderson, H., and J. Jackson (1987), Active tectonics of the Adriatic region, *Geophys. J. Int.*, *91*(3), 937–983, doi:10.1111/j.1365-246X.1987.tb01675.x.

Angelier, J., N. Lyberis, X. Le Pichon, E. Barrier, and P. Huchon (1982), The tectonic development of the Hellenic Arc and the Sea of the Crete: A synthesis (Mediterranean), *Tectonophysics*, *86*(1–3), 159–196, doi:10.1016/0040-1951(82)90066-X.

Armijo, R., H. Lyon-Caen, and D. Papanastassiou (1991), A possible normal-fault rupture for the 464 BC Sparta earthquake, *Nature*, *351*, 137–139, doi:10.1038/351137a0.

Armijo, R., H. Lyon-Caen, and D. Papanastassiou (1992), East-west extension and Holocene normal-fault scarps in the Hellenic Arc, *Geology*, *20*(6), 491–494, doi:10.1130/0091-7613(1992)020<0491:EWEAHN>2.3.CO;2.

Battaglia, M., M. H. Murray, E. Serpelloni, and R. Bürgmann (2004), The Adriatic region: An independent microplate within the Africa-Eurasia collision zone, *Geophys. Res. Lett.*, *31*, L09605, doi:10.1029/2004GL019723.

Beißer, M., M. Wyss, and R. Kind (1990), Inversion of source parameters for subcrustal earthquakes in the Hellenic Arc, *Geophys. J. Int.*, *103*(2), 439–450, doi:10.1111/j.1365-246X.1990.tb01783.x.

Benetatos, C., A. Kiratzi, C. Papazachos, and G. Karakaisis (2004), Focal mechanisms of shallow and intermediate depth earthquakes along the Hellenic Arc, *J. Geodyn.*, *37*(2), 253–296, doi:10.1016/j.jog.2004.02.002.

Benetatos, C., A. Kiratzi, A. Ganas, M. Ziazia, A. Plessa, and G. Drakatos (2006), Strike-slip motions in the Gulf of Sığaçik (western Turkey): Properties of the 17 October 2005 earthquake seismic sequence, *Tectonophysics*, *426*(3–4), 263–279, doi:10.1016/j.tecto.2006.08.003.

Birch, F. (1966), Compressibility; elastic constants, in *Handbook of Physical Constants*, edited by S. P. Clark Jr., in *Mem. Geol. Soc. Am.*, *97*, 97–173.

Bird, P., and Y. Y. Kagan (2004), Plate-tectonic analysis of shallow seismicity: apparent boundary width, beta, corner magnitude, coupled lithosphere thickness, and coupling in seven tectonic settings, *Bull. Seismol. Soc. Am.*, *94*, 2380–2399, doi:10.1785/0120030107.

Bohnhoff, M., J. Makris, D. Papanikolaou, and G. Stavrakakis (2001), Crustal investigation of the Hellenic subduction zone using wide aperture seismic data, *Tectonophysics*, *343*(3–4), 239–262, doi:10.1016/S0040-1951(01)00264-5.

Brooks, M., and G. Ferentinos (1980), Structure and evolution of the Sporadhes basin of the North Aegean trough, northern Aegean Sea, *Tectonophysics*, *68*(1–2), 15–30, doi:10.1016/0040-1951(80)90006-2.

Brune, J. N., and W. Thatcher (2002), Strength and energetics of active fault zones, in *International Handbook of Earthquake and Engineering Seismology*, *Int. Geophys. Ser.*, vol. 81, edited by W. H. K. Lee et al., pp. 569–588, Academic, Amsterdam.

Caputo, R., C. Monaco, and L. Tortorici (2006), Multiseismic cycle deformation rates from Holocene normal fault scarps on Crete (Greece), *Terra Nova*, *18*, 181–190, doi:10.1111/j.1365-3121.2006.00678.x.

Cattin, R., H. Lyon-Caen, and J. Chéry (1997), Quantification of interplate coupling in subduction zones and forearc topography, *Geophys. Res. Lett.*, *24*, 1563–1566, doi:10.1029/97GL01550.

Chamot-Rooke, N., A. Rabaute, and C. Kreemer (2005), Western Mediterranean Ridge mud belt correlates with active shear strain at the prism-backstop geological contact, *Geology*, *33*, 861–864, doi:10.1130/G21469.1.

Chlieh, M., J. B. de Chabalier, J. C. Ruegg, R. Armijo, R. Dmowska, J. Campos, and K. L. Feigl (2004), Crustal deformation and fault slip during the seismic cycle in the North Chile subduction zone, from GPS and InSAR observations (p 695–711), *Geophys. J. Int.*, doi:10.1111/j.1365-246X.2004.02326.x.

Christensen, N. I. (1996), Poisson's ration and crustal seismology, *J. Geophys. Res.*, *101*, 3139–3156, doi:10.1029/95JB03446.

Christensen, N. I., and W. D. Mooney (1995), Seismic velocity structure and composition of the continental crust: A global view, *J. Geophys. Res.*, *100*, 3047–3054.

Cianetti, S., P. Gasperini, C. Giunchi, and E. Boschi (2001), Numerical modelling of the Aegean-Anatolian region: Geodynamical constraints from observed rheological heterogeneities, *Geophys. J. Int.*, *146*, 760–780, doi:10.1046/j.1365-246X.2001.00492.x.

de Chabalier, J. B., H. Lyon-Caen, A. Zollo, A. Deschamps, P. Bernard, and D. Hatzfeld (1992), A detailed analysis of microearthquakes in western Crete from digital three-component seismograms, *Geophys. J. Int.*, *110*(2), 347–360, doi:10.1111/j.1365-246X.1992.tb00879.x.

De Martini, P. M., D. Pantosti, N. Palyvos, F. Lemeille, L. McNeill, and R. Collier (2004), Slip rates of the Aigion and Eliki Faults from uplifted marine terraces, Corinth Gulf, Greece, *C. R. Geosci.*, *336*(4–5), 325–334, doi:10.1016/j.crte.2003.12.006.

Faccenna, C., O. Bellier, J. Martinod, C. Piromallo, and V. Regard (2006), Slab detachment beneath eastern Anatolia: A possible cause for the formation of the North Anatolian fault, *Earth Planet. Sci. Lett.*, *242*, 85–97, doi:10.1016/j.epsl.2005.11.046.

Fassoulas, C. (2001), The tectonic development of a Neogene graben at the leading edge of the active European margin, The Heraklion basin, Crete, Greece, *J. Geodyn.*, *31*, 49–70, doi:10.1016/S0264-3707(00)00017-X.

Fernandes, R. M. S., B. A. C. Ambrosius, R. Noomen, L. Bastos, M. J. R. Wortel, W. Spakman, and R. Govers (2003), The relative motion between Africa and Eurasia as derived from ITRF2000 and GPS data, *Geophys. Res. Lett.*, *30*(16), 1828, doi:10.1029/2003GL017089.

Flemming, N. C. (1978), Holocene eustatic changes and coastal tectonics in the north-east Mediterranean: Implications for models of crustal consumption, *Philos. Trans. R. Soc. London, Ser. A*, *289*, 405–458, doi:10.1098/rsta.1978.0065.

Fortuin, A. R. (1978), Late Cenozoic history of eastern Crete and implications for the geology and geodynamics of the southern Aegean area, *Geol. Mijnbouw*, *57*, 451–464.

Ganas, A., G. Drakatos, S. B. Pavlides, G. N. Stavrakakis, M. Ziazia, E. Sokos, and V. K. Karastathis (2005), The 2001 Mw = 6.4 Skyros earthquake, conjugate strike-slip faulting and spatial variation in stress within the central Aegean Sea, *J. Geodyn.*, *39*(1), 61–77, doi:10.1016/j.jog.2004.09.001.

Ganas, A., E. Serpelloni, G. Drakatos, M. Kolligri, I. Adamis, C. Tsimi, and E. Batsi (2009), The Mw 6.4 SW-Achaia (western Greece) earthquake of 8 June 2008: Seismological, field, GPS observations and stress modeling, *J. Earthquake Eng.*, in press.

Gautier, P., J.-P. Brun, R. Moriceau, D. Sokoutis, J. Martinod, and L. Jolivet (1999), Timing, kinematics and cause of Aegean extension: A scenario based on a comparison with simple analogue experiments, *Tectonophysics*, *315*(1–4), 31–72, doi:10.1016/S0040-1951(99)00281-4.

Giunchi, C., A. Kiratzi, R. Sabadini, and E. Louvari (1996), A numerical model of the Hellenic subduction zone: Active stress field and sea-level changes, *Geophys. Res. Lett.*, *23*(18), 2485–2488, doi:10.1029/96GL02166.

Guidoboni, E., and A. Comastri (1997), The large earthquake of 8 August 1303 in Crete: Seismic scenario and tsunami in the Mediterranean area, *J. Seismol.*, *1*, 55–72, doi:10.1023/A:1009737632542.

Hamouda, A. Z. (2006), Seismic hazard of the eastern Mediterranean, *Acta Geophys.*, *54*, 165–176, doi:10.2478/s11600-006-0013-z.

Hatzfeld, D., M. Bernard, K. Makropoulos, and P. Hatzidimitriou (1993), Microearthquake seismicity and fault-plane solutions in the southern Aegean and its geodynanic implications, *Geophys. J. Int.*, *115*(3), 799–818, doi:10.1111/j.1365-246X.1993.tb01493.x.

Hollenstein, C., M. D. Müller, A. Geiger, and H.-G. Kahle (2008), Crustal motion and deformation in Greece from a decade of GPS measurements, 1993–2003, *Tectonophysics*, *449*, 17–40, doi:10.1016/j.tecto.2007.12.006.

Houghton, S. L., G. P. Roberts, I. D. Papanikolaou, J. M. McArthur, and M. A. Gilmour (2003), New ^{234}U-^{230}Th coral dates from the western Gulf of Corinth: Implications for extensional tectonics, *Geophys. Res. Lett.*, *30*(19), 2013, doi:10.1029/2003GL018112.

Husson, L. (2006), Dynamic topography above retreating subduction zones, *Geology*, *34*, 741–744, doi:10.1130/G22436.1.

Hutton, W., C. DeMets, O. Sánchez, G. Suárez, and J. Stock (2001), Slip kinematics and dynamics during and after the 1995 October 9 Mw = 8.0 Colima-Jalisco earthquake, Mexico, from GPS geodetic constraints, *Geophys. J. Int.*, *146*(3), 637–658, doi:10.1046/j.1365-246X.2001.00472.x.

Jackson, J. A., and D. McKenzie (1984), Active tectonics of the Alpine-Himalayan Belt between western Turkey and Pakistan, *Geophys. J. Int.*, *77*(1), 185–264, doi:10.1111/j.1365-246X.1984.tb01931.x.

Jackson, J. A., J. Gagnepain, G. Houseman, G. C. P. King, P. Papadimitriou, C. Soufleris, and J. Virieux (1982), Seismicity, normal faulting, and the geomorphological development of the Gulf of Corinth (Greece): The Corinth earthquakes of February and March 1981, *Earth Planet. Sci. Lett.*, *57*(2), 377–397, doi:10.1016/0012-821X(82)90158-3.

Kershaw, S., L. Guo, and J. C. Braga (2005), A Holocene coral-algal reef at Mavra Litharia, Gulf of Corinth, Greece: Structure, history, and applications in relative sea-level change, *Mar. Geol.*, *215*(3–4), 171–192, doi:10.1016/j.margeo.2004.12.003.

Kiratzi, A., and E. Louvari (2003), Focal mechanisms of shallow earthquakes in the Aegean Sea and the surrounding lands determined by waveform modeling: A new database, *J. Geodyn.*, *36*, 251–274, doi:10.1016/S0264-3707(03)00050-4.

Kiratzi, A. A., G. S. Wagner, and C. A. Langston (1991), Source parameters of some large earthquakes in northern Aegean determined by body waveform inversion, *Pure Appl. Geophys.*, *135*(4), 515–527, doi:10.1007/BF01772403.

Kokkalas, S., and T. Doutsos (2001), Strain-dependent stress field and plate motions in the south-east Aegean region, *J. Geodyn.*, *32*, 311–332, doi:10.1016/S0264-3707(01)00035-7.

Kopf, A., and K. M. Brown (2003), Friction experiments on saturated sediments and their implications for the stress state of the Nankai and Barbados subduction thrusts, *Mar. Geol.*, *202*, 193–210, doi:10.1016/S0025-3227(03)00286-X.

Kreemer, C., and N. Chamot-Rooke (2004), Contemporary kinematics of the southern Aegean and the Mediterranean Ridge, *Geophys. J. Int.*, *157*, 1377–1392, doi:10.1111/j.1365-246X.2004.02270.x.

Laigle, M., M. Sachpazi, and A. Hirn (2004), Variation of seismic coupling with slab detachment and upper plate structure along the western Hellenic subduction zone, *Tectonophysics*, *391*(1–4), 85–95, doi:10.1016/j.tecto.2004.07.009.

Le Pichon, X. (1983), Land-locked oceanic basins and continental collision: The Eastern Mediterranean as a case example, in *Mountain Building Processes*, edited by K. J. Hsü, pp. 201–211, Academic, London.

Le Pichon, X., and J. Angelier (1981), The Aegean Sea, *Philos. Trans. R. Soc. London, Ser. A*, *300*, 357–372, doi:10.1098/rsta.1981.0069.

Li, X., G. Bock, A. Vafidis, R. Kind, H.-P. Harjes, W. Hanka, K. Wylegalla, and X. Yuan (2003), Receiver function study of the Hellenic subduction zone: Imaging crustal thickness variations and the oceanic Moho of the descending African lithosphere, *Geophys. J. Int.*, *155*(2), 733–748, doi:10.1046/j.1365-246X.2003.02100.x.

Lorito, S., et al. (2008), Earthquake-generated tsunamis in the Mediterranean sea: Scenarios of potential threats to southern Italy, *J. Geophys. Res.*, *113*(B1), B01301, doi:10.1029/2007JB004943.

Lyon-Caen, H., et al. (1988), The 1986 Kalamata (south Peloponnese) earthquake: Detailed study of a normal fault, evidences for east-west extension in the Hellenic Arc, *J. Geophys. Res.*, *93*, 14,967–15,000, doi:10.1029/JB093iB12p14967.

Mascle, J., and L. Martin (1990), Shallow structure and recent evolution of the Aegean Sea: A synthesis based on continuous reflection profiles, *Mar. Geol.*, *94*(4), 271–299, doi:10.1016/0025-3227(90)90060-W.

McKenzie, D. (1972), Active tectonics of the Mediterranean region, *Geophys. J. R. Astron. Soc.*, *30*, 109–185.

Meghraoui, M., B. Delouis, M. Ferry, D. Giardini, P. Huggenberger, I. Spottke, and M. Granet (2001), Active normal faulting in the upper Rhine graben and paleoseismic identification of the 1356 Basel earthquake, *Science*, *293*(5537), 2070–2073, doi:10.1126/science.1010618.

Meier, T., K. Dietrich, B. Stockhert, and H.-P. Harjes (2004), One-dimensional models of shear wave velocity for the eastern Mediterranean obtained from the inversion of Rayleigh wave phase velocities and tectonic implications, *Geophys. J. Int.*, *156*(1), 45–58, doi:10.1111/j.1365-246X.2004.02121.x.

Meier, T., D. Becker, B. Endrun, M. Rische, M. Bohnhoff, B. Stöckhert, and H.-P. Harjes (2007), A model for the Hellenic subduction zone in the area of Crete based on seismological investigations, in *Late Palaeozoic and Mesozoic Ecosystems in SE Asia*, edited by E. Buffetaut, J. Le Loeuff, and V. Suteethorn, *Geol. Soc. Spec. Publ.*, *291*, 183–199, doi:10.1144/SP291.9.

Meijer, P. T., and M. J. R. Wortel (1997), Present-day dynamics of the Aegean region: A model analysis of the horizontal pattern of stress and deformation, *Tectonics*, *16*, 879–895, doi:10.1029/97TC02004.

Meulenkamp, J. E., G. J. van der Zwaan, and W. A. van Wamel (1994), On late Miocene to recent vertical motions in the Cretan segment of the Hellenic Arc, *Tectonophysics*, *234*(1–2), 53–72, doi:10.1016/0040-1951(94)90204-6.

Meyer, B., R. Armijo, D. Massonnet, J. B. De Chabalier, C. Delacourt, J. C. Ruegg, J. Achache, P. Briole, and D. Papanastassiou (1996), The 1995 Grevena (northern Greece) earthquake: Fault model constrained with tectonic observations and SAR interferometry, *Geophys. Res. Lett.*, *23*(19), 2677–2680, doi:10.1029/96GL02389.

Nyst, M., and W. Thatcher (2004), New constraints on the active tectonic deformation of the Aegean, *J. Geophys. Res.*, *109*, B11406, doi:10.1029/2003JB002830.

Okada, Y. (1992), Internal deformation due to shear and tensile faults in a half space, *Bull. Seismol. Soc. Am.*, *82*, 1018–1040.

Okay, A. I., and M. Satir (2000), Coeval plutonism and metamorphism in a latest Oligocene metamorphic core complex in northwest Turkey, *Geol. Mag.*, *137*(5), 495–516, doi:10.1017/S0016756800004532.

Papadimitriou, E. E., and V. G. Karakostas (2008), Rupture model of the great AD 365 Crete earthquake in the southwestern part of the Hellenic Arc, *Acta Geophys.*, *56*(2), 293–312, doi:10.2478/s11600-008-0001-6.

Papanikolaou, D. J., and L. H. Royden (2007), Disruption of the Hellenic Arc: Late Miocene extensional detachment faults and steep Pliocene-Quaternary normal faults—Or what happened at Corinth?, *Tectonics*, *26*, TC5003, doi:10.1029/2006TC002007.

Papazachos, B. C., D. G. Panagiotopoulos, T. M. Tsapanos, D. M. Mountrakis, and G. C. Dimopoulos (1983), A study of the 1980 summer seismic sequence in the Magnesia region of Central Greece, *Geophys. J. Int.*, *75*(1), 155–168, doi:10.1111/j.1365-246X.1983.tb01883.x.

Papazachos, C., P. Hatzidimitriou, D. Panagiotopoulos, and G. Tsokas (1995), Tomography of the crust and upper mantle in southeast Europe, *J. Geophys. Res.*, *100*, 12,405–12,422, doi:10.1029/95JB00669.

Papazachos, B. C., V. G. Karakostas, C. B. Papazachos, and E. M. Scordilis (2000a), The geometry of the Wadati-Benioff zone and lithospheric kinematics in the Hellenic Arc, *Tectonophysics*, *319*(4), 275–300, doi:10.1016/S0040-1951(99)00299-1.

Papazachos, B. C., P. E. Comninakis, G. F. Karakaisis, B. G. Karakostas, C. A. Papaioannou, C. B. Papazachos, and E. M. Scordilis (2000b), A catalogue of earthquakes in Greece and surrounding area for the period 550BC–1999, *Publ. 1*, 333 pp., Geophys. Lab., Univ. of Thessaloniki, Thessaloniki, Greece.

Pavlides, S. B., and M. D. Tranos (1991), Structural characteristics of 2 strong earthquakes in the north-Aegean—Ierissos (1932) and Agios-Efstratios, 1968, *J. Struct. Geol.*, *13*(2), 205–214, doi:10.1016/0191-8141(91)90067-S.

Pirazzoli, P. A., J. Thommeret, Y. Thommeret, J. Laborel, and L. F. Montaggioni (1982), Crustal block movements from Holocene shorelines: Crete and Antikythira (Greece), *Tectonophysics*, *86*(1–3), 27–43, doi:10.1016/0040-1951(82)90060-9.

Pirazzoli, P. A., L. F. Montaggioni, J. F. Saliège, G. Segonzac, Y. Thommeret, and C. Vergnaud-Grazzini (1989), Crustal block movements from Holocene shorelines: Rhodes Island (Greece), *Tectonophysics*, *170*(1–2), 89–114, doi:10.1016/0040-1951(89)90105-4.

Pirazzoli, P. A., J. Laborel, and S. C. Stiros (1996), Earthquake clustering in the eastern Mediterranean during historical times, *J. Geophys. Res.*, *101*(B3), 6083–6097, doi:10.1029/95JB00914.

Pirazzoli, P. A., S. C. Stiros, M. Fontugne, and M. Arnold (2004), Holocene and Quaternary uplift in the central part of the southern coast of the Corinth Gulf (Greece), *Mar. Geol.*, *212*(1–4), 35–44, doi:10.1016/j.margeo.2004.09.006.

Poppe, L. J., S. J. Williams, and V. F. Paskevich (Eds.) (2005), U.S. Geological Survey East-Coast sediment analysis: Procedures, database, and GIS data, *U.S. Geol. Surv. Open File Rep., 2005-1001*.

Price, S., T. Higham, L. Nixon, and J. Moody (2002), Relative sea-level changes in Crete: Reassessment of radiocarbon dates from Sphakia and west Crete, *Annu. Br. Sch. Athens*, *97*, 171–200.

Regard, V., C. Faccenna, J. Martinod, and O. Bellier (2005), Slab pull and indentation tectonics: Insights from 3D laboratory experiments, *Phys. Earth Planet. Inter.*, *149*, 99–113, doi:10.1016/j.pepi.2004.08.011.

Reilinger, R., et al. (2006), GPS constraints on continental deformation in the Africa-Arabia-Eurasia continental collision zone and implications for the dynamics of plate interactions, *J. Geophys. Res.*, *111*, B05411, doi:10.1029/2005JB004051.

Ring, U., and T. Reischmann (2002), The weak and superfast Cretan detachment, Greece: Exhumation at subduction rates in extruding wedges, *J. Geol. Soc.*, *159*, 225–228, doi:10.1144/0016-764901-150.

Roberts, G. P., and A. Ganas (2000), Fault-slip directions in central and southern Greece measured from striated and corrugated fault planes: Comparison with focal mechanism and geodetic data, *J. Geophys. Res.*, *105*, 23,443–23,462, doi:10.1029/1999JB900440.

Ruff, L. J. (2002), State of stress within the Earth, in *International Handbook of Earthquake and Engineering Seismology*, *Int. Geophys. Ser.*, vol. 81, edited by W. H. K. Lee et al., pp. 539–557, Academic, Amsterdam.

Sachpazi, M., A. Galvé, M. Laigle, A. Hirn, E. Sokos, A. Serpetsidaki, J.-M. Marthelot, J. M. Pi Alperin, B. Zelt, and B. Taylor (2007), Moho topography under central Greece and its compensation by Pn time-terms for the accurate location of hypocenters: The example of the Gulf of Corinth 1995 Aigion earthquake, *Tectonophysics*, *440*(1–4), 53–65, doi:10.1016/j.tecto.2007.01.009.

Scordilis, E. M., G. F. Karakaisis, B. G. Karacostas, D. G. Panagiotopoulos, P. E. Comninakis, and B. C. Papazachos (1985), Evidence for transform faulting in the Ionian sea: The Cephalonia island earthquake sequence of 1983, *Pure Appl. Geophys.*, *123*(3), 388–397, doi:10.1007/BF00880738.

Serpelloni, E., M. Anzidei, P. Baldi, G. Casula, and A. Galvani (2005), Crustal velocity and strain-rate fields in Italy and surrounding regions: New results from the analysis of permanent and non-permanent GPS networks, *Geophys. J. Int.*, *161*(3), 861–880, doi:10.1111/j.1365-246X.2005.02618.x.

Seyitoglu, G., and B. C. Scott (1992), Late Cenozoic volcanic evolution of the northeastern Aegean region, *J. Volcanol. Geotherm. Res.*, *54*(1–2), 157–176, doi:10.1016/0377-0273(92)90121-S.

Shaw, B., N. N. Ambraseys, P. C. England, M. A. Floyd, G. J. Gorman, T. F. G. Higham, J. A. Jackson, J. M. Nocquet, C. C. Pain, and M. D. Piggott (2008), Eastern Mediterranean tectonics and tsunami hazard inferred from the AD 365 earthquake, *Nat. Geosci.*, *1*(4), 268–276, doi:10.1038/ngeo151.

Snopek, K., T. Meier, B. Endrun, M. Bohnhoff, and U. Casten (2007), Comparison of gravimetric and seismic constraints on the structure of the Aegean lithosphere in the forearc of the Hellenic subduction zone in the area of Crete, *J. Geodyn.*, *44*(3–5), 173–185, doi:10.1016/j.jog.2007.03.005.

Spakman, W., M. J. R. Wortel, and N. J. Vlaar (1988), The Hellenic subduction zone: A tomographic image and its geodynamic implications, *Geophys. Res. Lett.*, *15*(1), 60–63, doi:10.1029/GL015i001p00060.

Stein, R. S., G. C. P. King, and J. B. Rundle (1988), The growth of geological structures by repeated earthquakes: 2. Field examples of continental dip-slip faults, *J. Geophys. Res.*, *93*, 13,319–13,331, doi:10.1029/JB093iB11p13319.

Stiros, S. C., J. Laborel, F. Laborel-Deguen, S. Papageorgiou, J. Evin, and P. A. Pirazzoli (2000), Seismic coastal uplift in a region of subsidence: Holocene raised shorelines of Samos Island, Aegean Sea, Greece, *Mar. Geol.*, *170*(1–2), 41–58, doi:10.1016/S0025-3227(00)00064-5.

Stiros, S. C. (2001), The AD 365 Crete earthquake and possible seismic clustering during the fourth to sixth centuries AD in the eastern Mediterranean: A review of historical and archaeological data, *J. Struct. Geol.*, *23*, 545–562, doi:10.1016/S0191-8141(00)00118-8.

Subarya, C., et al. (2006), Plate-boundary deformation associated with the great Sumatra-Andaman earthquake, *Nature*, *440*(7080), 46–51, doi:10.1038/nature04522.

Taymaz, T., J. A. Jackson, and R. Westaway (1990), Earthquake mechanisms in the Hellenic Trench near Crete, *Geophys. J. Int.*, *102*, 695–731, doi:10.1111/j.1365-246X.1990.tb04590.x.

Taymaz, T., J. A. Jackson, and D. McKenzie (1991), Active tectonics of the north and central Aegean Sea, *Geophys. J. Int.*, *106*, 433–490, doi:10.1111/j.1365-246X.1991.tb03906.x.

van der Meijde, M., S. van der Lee, and D. Giardini (2003), Crustal structure beneath broad-band seismic stations in the Mediterranean region, *Geophys. J. Int.*, *152*(3), 729–739, doi:10.1046/j.1365-246X.2003.01871.x.

Vigny, C., et al. (2005), Insight into the 2004 Sumatra-Andaman earthquake from GPS measurements in southeast Asia, *Nature*, *436*(7048), 201–206, doi:10.1038/nature03937.

Wortel, M. J. R., and W. Spakman (2000), Subduction and slab detachment in the Mediterranean-Carpathian region, *Science*, *290*, 1910–1917, doi:10.1126/science.290.5498.1910.

Yolsal, S., T. Taymaz, and A. C. Yalçiner (2007), Understanding tsunamis, potential source regions and tsunami-prone mechanisms in the Eastern Mediterranean, in *Late Palaeozoic and Mesozoic Ecosystems in SE Asia*, edited by E. Buffetaut, J. Le Loeuff, and V. Suteethorn, *Geol. Soc. Spec. Publ.*, *291*, 201–230, doi:10.1144/SP291.10.

A. Ganas, Geodynamics Institute, National Observatory of Athens, Lofos Nymfon, P.O. Box 20048, G-11810 Athens, Greece. (aganas@gein.noa.gr)

T. Parsons, U.S. Geological Survey, 345 Middlefield Road, MS 977, Menlo Park, CA 94025, USA. (tparsons@usgs.gov)